Caveolin-1 isoform reorganization studied by image correlation spectroscopy

Anja Nohe,†[a] Eleonora Keating,†[a] Crystal Loh,[a] Michael T. Underhill[b] and Nils O. Petersen*[a]

[a] *Department of Chemistry, University of Western Ontario, London, Canada N6A1B7. E-mail: petersen@uwo.ca; Fax: (519) 661 3022; Tel: (519) 661 2111 ext 86333*
[b] *School of Dentistry, University of Western Ontario, London, Canada N6A6C1*

Received 2nd May 2003, Accepted 11th July 2003
First published as an Advance Article on the web 15th October 2003

Caveolae are small, flask shaped invaginations in the cell membrane. They are thought to play a crucial role in cell signaling, endocytosis and intracellular cholesterol transport. Caveolin-1, 2 and 3 are key proteins, which are important for the formation of the invaginations on the cell surface. Caveolin-1 exists in two isoforms: caveolin-1 alpha (α) and caveolin-1 beta (β). Little is known about the difference between these two isoforms, and less in known about their role in cell signaling. Bone morphogenetic proteins (BMPs) are a subfamily of the TGF beta superfamily and their response is mediated by serine/threonine kinase receptors. Epidermal growth factor (EGF) is known to signal through tyrosine kinase receptors of the ErbB family. Here we report on the aggregation and association of caveolin-1 isoforms with these receptors and the effect of BMP and EGF activation on caveolin-1 distribution in A431 cells. Our data, obtained by application of a family of image correlation spectroscopy tools, indicate that BMP and EGF stimulation lead to a rearrangement of the caveolin-1 isoforms on the cell surface. BMP as well as EGF stimulation leads to a rearrangement of the caveolin-1 β isoform into domains enriched in the caveolin-1 α isoform. We further show that about 20–30% of the caveolin-1 present at the surface of the cells co-localize with the EGF and BMP receptors. Using a reporter gene assay sensitive to the activation of the BMP pathway, we show that overexpression of caveolin-1 β inhibits signaling. Our data suggest that the two isoforms of caveolin-1 play different roles on the cell surface and that caveolae are dynamic structures.

Introduction

Caveolae are small, flask-shaped invaginations of the cell membrane, which are thought to play a crucial role in endocytosis, signaling and intracellular cholesterol transport.[1–3] Caveolin-1, 2 and 3 are the key proteins involved in the formation of the invaginations.[4–6] Caveolin-1 is expressed in two isoforms, caveolin-1 α and caveolin-1 β, that differ in their coding. Still, the two caveolin-1 isoforms have a common hydrophobic stretch of amino acids, a scaffolding domain and an

† Both authors contributed equally.

This journal is © The Royal Society of Chemistry 2003

acetylated C-terminus.[7,8] They are distributed slightly differently on the cell surface, and previous work suggests that there are caveolae composed only (or mainly) of the β isoform as well as caveolae with both isoforms present.[9]

Bone morphogenetic proteins (BMPs) play crucial roles during embryonic development in chondrogenesis, osteogenesis, neurogenesis and hematopoiesis.[10–17] They exert their function by signaling through serine threonine kinase receptors. BMPs need to bind to at least one type-I and one type-II receptor in order to activate the Smad or p38 pathways.[18–28]

Epidermal growth factor (EGF) is in part responsible for the proliferation of cells and exerts its function by signaling through tyrosine kinase receptors, leading to the activation of the Map kinase (Mapk) pathways.[29–31]

There is increasing evidence that domains on the cell surface exist to act as sites for protein–protein interactions leading to activation of specific signaling pathways. By serving as regions of the cell surface that can be enriched in receptors to signaling proteins, the probability of interaction among the receptors increases significantly allowing for more rapid responses. In the case of the BMP receptors, their organization in caveolae may facilitate creation of preformed complexes of type-I and type II receptors. Interactions between receptors and regulatory proteins within the domains can, in principle, lead to either activation or inhibition of the corresponding signaling pathways. However, unless the caveolae are specific to particular receptor families, the high density of receptors in the domain could lead to interaction between different receptor systems and hence cross-talk between otherwise distinct signaling pathways. It is, therefore, important to study protein–protein interactions within these domains and to determine whether these interactions can change.

Generally, we aim to understand whether stimulation of a cell with receptor specific ligands influences the receptor distribution or the caveolin composition within the caveolae. In this work, we investigate the association of caveolin-1 isoforms with the BMP receptors of type-II (BRII) and type-Ia (BRIa) and with the EGF receptor, ErbB1. We apply image correlation spectroscopy techniques to determine quantitatively the density of the receptors and the caveolin-1 isotypes as well as the extent to which they co-localize.

Materials and methods

Materials

Recombinant BMP-2 was obtained from Wyeth (Boston, NY, USA) and human recombinant EGF was purchased from Sigma (St. Louis, MO, USA). The polyclonal antisera against the BMP receptors, BRIa and BRII, and the polyclonal antibody against the EGF receptor were from Santa Cruz (Santa Cruz, CA, USA). The antibodies recognizing only caveolin-1 α (clone 2234) or both of the caveolin-1 α and β isoforms (clone 2297) were purchased from Transduction Laboratories (New York, NY, USA). The secondary antibodies, donkey anti-goat RRX and goat anti-mouse Alexa Fluor 488, were purchased from Molecular Probes (Eugene, OR, USA). The A431 cell line (CRL 1555) was purchased from American Type Culture Collection (Manassa, VA, USA).). The plasmid encoding GFP-tagged caveolin-1 β was provided by Dr H. Kogo (Department of Anatomy, Nagoya University School of Medicine, Showa-ku, Nagoya, 466-8550, Japan.)

Immunofluorescence labeling of cell surface receptors

To measure the distribution of the caveolin-1 on the cell surface, we employed ICS and ICCS measurements, which require acquisition of high quality fluorescence images with a laser scanning confocal microscope. Normal A431 cells were grown on 22 mm coverslips. Following 72 h of serum-starvation, the A431 cells were stimulated, or not stimulated, with 20 nM BMP-2 for 2.5 h or 100 ng mL^{-1} EGF for 30 min and fixed using acetone/methanol fixation.[32] After blocking for 30 min with 5% BSA, the cells were incubated with polyclonal antisera recognizing either BRII or BRIa, with polyclonal antibody recognizing the EGFR, or with antibodies recognizing caveolin-1 α (clone 2234) or caveolin-1 α and β (clone 2297) according to manufacturers protocols. The

cells were washed 3 times with PBS for 5 min and afterwards, they were incubated with the corresponding fluorescently tagged secondary antibodies at a concentration of 20 μg mL^{-1}. Cells were washed again three times for 5 min with PBS and the coverslips were mounted on airvol and dried overnight.

Luciferase reporter assay

A431 cells grown in 60 mm dishes were co-transfected with the plasmid containing a Smad Binding Element (pSBE), which is sensitive to the activation of the BMP signaling pathway, a *Renilla* luciferase reporter construct (which is used for normalization of the chemiluminescence response) and the caveolin-1 β construct using Fugene6 (Boehringer). After transfection, the cells were stimulated, or not stimulated, for 12 h with 20 nM BMP-2, lysed and the luciferase activity was measured using a dual luciferase assay system (Promega, Madison, WI, USA).

Confocal microscopy

Labeled cells were visualized using a Biorad MRC 600 confocal microscope equipped with an Ar/Kr mixed gas laser and using the appropriate filter sets for dual fluorophore imaging. Cells expressing the receptors were selected under mercury lamp illumination using a 60 × (1.4 numerical aperture) objective on an inverted Nikon microscope. An area on the cell, removed from the nucleus, was enlarged and recorded at the zoom 10 setting. The filter wheel was set for 488 nm laser excitation to measure Alexa Fluor 488 fluorescence, and neutral density filters were used to attenuate the laser to 1% laser power. Fifteen scans were accumulated on photomultiplier tube 2 (PMT2) in the photon counting mode (to ensure linear scaling of the intensity). The filter wheel was then shifted to allow excitation with the 568 nm laser line for Alexa Fluor 568 fluorescence, and 20 scans were accumulated on PMT1 for BMP receptors, whereas 9 scans were accumulated on PMT1 for the EGF receptor (EFGR). Each of the photomultiplier tubes were set to a black level of 6.0 on the vernier scale and a gain setting of 10. After collection of each set of images was finished, additional images were collected using identical settings but with the shutter to the sample closed to obtain a measure of the dark current for each PMT.

Correlation spectroscopy

Image correlation spectroscopy (ICS) and image cross-correlation spectroscopy (ICCS) are two techniques that can be used to study the distribution and localization of receptors.[33–38] The technique and selected applications have been presented previously at Faraday Discussion 111.[39] Here we provide a brief overview of the techniques and their interpretation.

Image correlation spectroscopy. ICS involves autocorrelation analysis of the intensity fluctuations within confocal images collected, in this case, from cells that contain immunofluorescently labeled proteins.

If the fluorescence intensity in a pixel, located at position (x,y) in the image, is $i(x,y)$, then the corresponding normalized fluorescence intensity fluctuation, $\delta i(x,y)$, is given by:

$$\delta i(x,y) = \frac{i(x,y) - \langle i(x,y)\rangle}{\langle i(x,y)\rangle} \tag{1}$$

The normalized spatial autocorrelation function, $g(\xi,\eta)$, is then given by:

$$g(\xi,\eta) = \langle \delta i(x,y)\delta i(x+\xi,y+\eta)\rangle \tag{2}$$

where the angular brackets indicate the average over all spatial coordinates and ξ and η are position lag coordinates for the x and y axes in the image. It is known that the limit of the autocorrelation function as ξ and η approach zero, $g(0,0)$, is equal to the variance of the normalized intensity fluctuations.[40] It is also known that for homogenous, non-interacting species, where the intensity is a true representation of the concentration, the variance of the normalized intensity

fluctuations is equal to the variance of the concentration fluctuations, which in turn is equal to the inverse of the number of particles in the observation area, $\bar{N}_p$.[41]

$$g(0,0) = \mathrm{var}(\delta i(x,y)) = \mathrm{var}(\delta c(x,y)) = \frac{1}{\bar{N}_p} \tag{3}$$

In practice, the two-dimensional autocorrelation function for the image is obtained by first calculating the Fourier transform of the image, then calculating the power spectrum (by multiplying the real and the imaginary components of the transform) and finally calculating the reverse Fourier transform. The resulting two-dimensional autocorrelation function is then fit to a two-dimensional gaussian function of known width (corresponding to the width of the laser beam at the focal point of confocal microscope). The amplitude of the function obtained from this fit gives the best estimate of $g(0,0)$ for that image.

Once the $g(0,0)$ value is known, an important parameter, called the cluster density (CD) can be calculated by eqn. (4). The CD value is an estimate of the average number of receptor clusters per unit area *i.e.*,

$$\mathrm{CD} = \frac{1}{g(0,0)\pi w^2} = \frac{\bar{N}_p}{\pi w^2} \tag{4}$$

Image cross correlation spectroscopy. Image cross-correlation spectroscopy (ICCS) is an extension of ICS. In ICCS, a cross-correlation function is also generated to measure the coincident fluorescence intensity fluctuations in images collected from two different chromophores attached to two different proteins or receptor types. One receptor type is labeled with a green probe and is imaged to give the intensity map, $i_g(x,y)$, while the second receptor type is labeled with a red probe and imaged to give the intensity map, $i_r(x,y)$. The normalized, spatial cross-correlation function can be calculated as:

$$g_{gr}(\xi,\eta) = \langle \delta i_g(x,y) \delta i_r(x+\xi, y+\eta) \rangle \tag{5}$$

In this case, the two-dimensional cross-correlation function is obtained by first calculating the Fourier transform of each of the two images, then cross-multiplying the real part from the green image with the imaginary part from the red image (or the imaginary part from the green image with the real part from the red image, the result is the same) and finally calculating the reverse Fourier transform of the 'mixed' power spectrum. The resulting cross-correlation function is fit to a two-dimensional gaussian as above to give the amplitude of the cross correlation function, $g_{gr}(0,0)$.

It has been shown for individual molecules that the zero-lag amplitude of the cross-correlation function reflects the extent of co-localization of the two chromophores on the cell surface.[35,36] We interpret the amplitude to reflect the average number of clusters with both chromophores present. Specifically:

$$g_{gr}(0,0) = \frac{\bar{N}_{gr}}{(\bar{N}_g + \bar{N}_{gr})\,(\bar{N}_r + \bar{N}_{gr})} = \bar{N}_{gr}\, g_g(0,0)\, g_r(0,0) \tag{6}$$

Here, $\bar{N}_g$, $\bar{N}_r$ and $\bar{N}_{gr}$ are the average number of clusters which are made up of only green labeled proteins, only red labeled proteins, and both green and red labeled proteins, respectively. Also, $g_g(0,0)$ and $g_r(0,0)$ are the autocorrelation functions corresponding to the individual green and red images. These are calculated from the individual images as indicated above.

By rearrangement, we can define a cluster density of co-localized chromophores as:

$$\mathrm{CD}_{gr} = \frac{g_{gr}(0,0)}{g_g(0,0)\, g_r(0,0)\, \pi w^2} = \frac{\bar{N}_{gr}}{\pi w^2} \tag{7}$$

The fraction of each protein type associated with the other type can finally be estimated by looking at the appropriate ratios of CD values:

$$F(\mathrm{g/r}) = \frac{\mathrm{CD}_{gr}}{\mathrm{CD}_g} \quad \text{or} \quad F(\mathrm{r/g}) = \frac{\mathrm{CD}_{gr}}{\mathrm{CD}_r} \tag{8}$$

In eqn. (8), $F(g/r)$ represents the fraction of green labeled protein clusters which contain red labeled proteins. Correspondingly, $F(r/g)$ is the fraction of red labeled protein clusters containing green labeled proteins.

It can be seen that ICCS provides quantitative information about the extent of co-localization of two different receptors, or in the current work, a receptor and a binding protein. The only caveat is that the interpretation of eqn. (6) is strictly only valid for individual chromophores.

Statistics

The experiments are designed to collect a large number of images, typically forty, each from a different cell in the sample. Past work indicates that the largest source of uncertainty in the ICS and ICCS measurements arises from variations between cells in a population. In order to obtain a reasonable estimate of the population properties (cluster density, fraction of co-localization) the data are pooled and averaged when more than one experiment is conducted. In all cases, the cluster density data are represented relative to the value for one, selected control experiment. All the data in a particular experiment are normalized to this same data set. The values of the standard error of the mean (SEM) were calculated from the raw data at the 95% confidence level. The significance of changes relative to the control was assessed by paired, two-tailed *t*-tests.

Results

Stimulation of A431 cells causes rearrangement of caveolin-1 isoforms

Normally cells are grown in a culture medium to which 10% fetal bovine serum is added. The serum provides some nutrients, but most importantly, a series of growth factors that stimulate cell proliferation. In the absence of the serum, cells divide less frequently, but grow well for up to one week. Removal of the serum, serum starvation, is used to isolate the effect of a specific growth factor on cell signaling, but can also affect the receptor concentration on the cell surface by up- or down-regulation at the gene expression level or through altered turn over through endocytosis. Specifically, serum starvation of A431 cells leads to the up-regulation of the BMP-type-II receptor within 72 h as seen by reverse transcription PCR (RT-PCR) and by immunofluorescence.[42] Further, starved A431 cells are sensitive to both BMP-2 and EGF stimulation whereas normal A431 cells are less sensitive to BMP-2 stimulation.

A431 cells were starved for 72 h and then stimulated (or not stimulated in control experiments) with the desired signaling protein. The cells were exposed to BMP-2 for 2.5 h or to 100 ng mL^{-1} of EGF for 30 min. The cells were then fixed and labeled for the caveolin-1 isoforms using a monoclonal antibody against caveolin-1 α or a monoclonal antibody recognizing both α and β isoforms followed by a secondary fluorescent antibody. Figs. 1A and 2A show representative confocal images at high magnification (zoom 10 provides 15.5 μm × 15.5 μm images). Forty high magnification images of flat regions of the cell surface were collected from forty separate cells and subjected to ICS analysis to provide a cluster density for each image (eqn. (4)). The average cluster density was calculated for this large number of images in order to obtain good population statistics.

Fig. 1B indicates that BMP-2 stimulation of starved A431 cells leads to a 39% decrease in the cluster density of caveolin-1 α and β as detected by labeling with the caveolin-1 antibody clone 2297 ($p = 8.75 \times 10^{-5}$). However, BMP-2 stimulation does not significantly change the cluster density of caveolin-1 α when detected alone by clone 2234 ($p = 0.97$). This suggests that the change in cluster density of caveolin-1 α and β arises from changes in the distribution of the caveolin-1 β isoform. Most likely, BMP-2 stimulation leads to a redistribution of the caveolin-1 β isoform into regions enriched in the α isoform, since the CD of caveolin-1 α and the CD of caveolin-1 α and β are not significantly different following the BMP-2 stimulation ($p = 0.14$).

Correspondingly, Fig. 2B shows that EGF stimulation leads to a 37% decrease in the cluster density of the caveolin-1 α and β isoform (detected by clone 2297) ($p = 0.013$) and that the stimulation with EGF does not significantly alter the cluster density of the caveolin-1 α isoform (detected by clone 2234) ($p = 0.96$). This observation is the same as that observed following BMP-2 stimulation. Thus, EGF stimulation leads to a redistribution of the caveolin-1 β isoform into

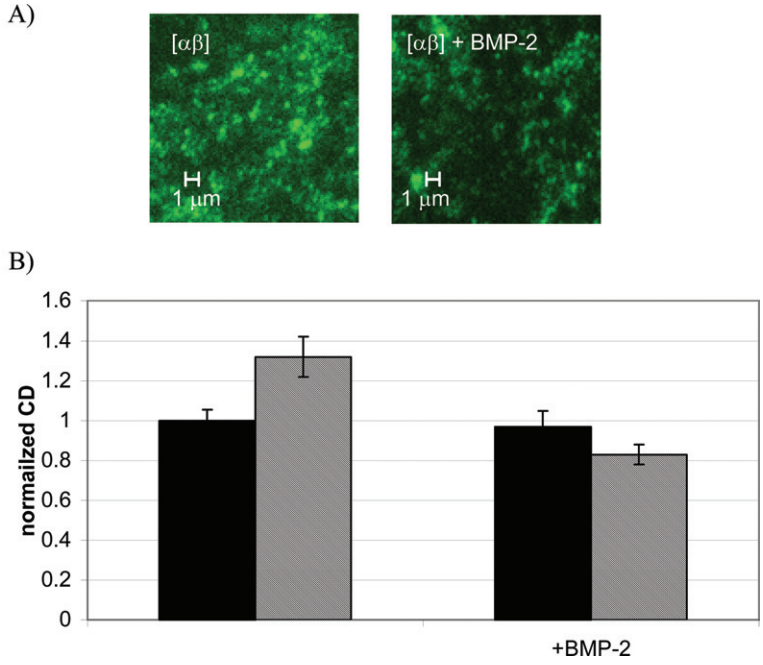

Fig. 1 A431 cells were cultured without serum. After 3 days, starved cells were stimulated, or not stimulated, with BMP-2, fixed and labeled for caveolin-1 α [α] or caveolin-1 α and β [αβ] using monoclonal antibodies against the caveolin-1 isoforms and a secondary fluorescently labeled antibody. Cell membrane expression was visualized by confocal microscopy. Forty images were collected at the highest magnification from forty different cells and the average intensity of the labeled caveolin-1 was calculated. For each image, the cluster density of each of the caveolin-1 isoforms was calculated by ICS (see methods) and expressed as a ratio relative to the cluster density observed for the antibodies recognizing caveolin-1 α and β. (A) High magnification fluorescent images of A431 cells with (right image) or without (left image) BMP-2 stimulation stained for caveolin-1 α and β (clone 2297). (B) Cluster densities of caveolin-1 α (clone 2234—solid bars) and caveolin-1 α and β (clone 2297—hatched bars) with (right panels) or without (left panels) BMP-2 stimulation.

regions enriched in the caveolin-1 α isoform, since the CD of cavolon-1 α and the CD of caveolin-1 α and β are not significantly changed following EGF stimulation ($p = 0.84$). Evidently, EGF and BMP-2 cause comparable changes in the caveolin isoform redistribution: in both cases the caveolin-1 β isoform is reorganized into domains enriched in caveolin-1 α following exposure to the signaling protein.

Caveolin-1 isoforms co-localize with BMP and EGF receptors

As described above, stimulation of A431 cells with BMP or EGF influences the aggregation of caveolin-1 β and appears to lead to changes in the composition of the caveolae. Since EGF and BMP mediate their signal through receptors that act respectively as serine threonine kinases or tyrosine kinases, it is likely that the influence on the caveolae compositions are caused by direct interactions with the caveolins, rather than through their respective signaling events. We, therefore, examined the extent of co-localization of the receptors with each of the caveolin-1 isoforms using image cross-correlation spectroscopy (ICCS).

Serum starved A431 cells, stimulated or not stimulated with BMP-2 or EGF, were fixed and the BMP receptors, EGF receptors and caveolin-1 isoforms were labeled using the specific antibodies against the proteins of interest and appropriate secondary fluorescent antibodies. The BMP and EGF receptors were labeled with donkey anti goat Alexa Fluor 568 conjugated secondary antibodies, whereas the caveolin-1 isoforms were labeled using goat anti mouse Alexa Fluor 488 secondary antibodies. Figs. 3A and 4A show representative examples of confocal images of selected, pair-wise labeling of a receptor and a caveolin-1 isoform. It is evident that the extent of

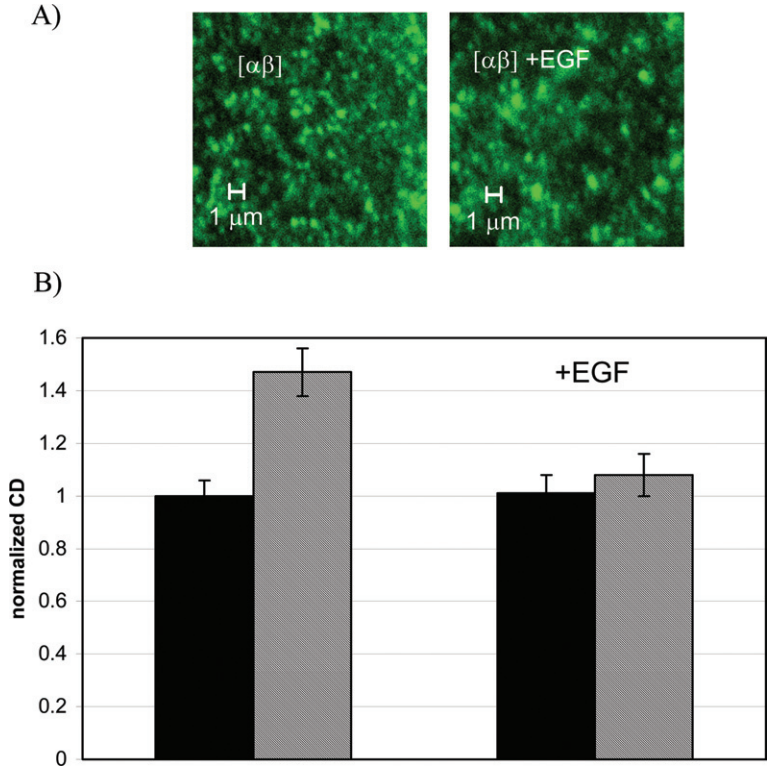

Fig. 2 A431 cells were serum starved for 72 h then stimulated, or not stimulated, with EGF, fixed and labeled for caveolin-1 α [α] or caveolin-1 α and β [αβ] using monoclonal antibodies against the caveolin-1 isoforms and a secondary fluorescently labeled antibody. Caveolin-1 expression on the cell membrane was visualized by confocal microscopy. Forty images were collected at the highest magnification from forty different cells and the average intensity of the labeled caveolin-1 was calculated. For each image, the cluster density of each of the caveolin-1 isoforms was calculated by ICS (see methods) and expressed as a ratio relative to the cluster density observed for the antibodies recognizing caveolin-1 α and β. (A) High magnification confocal images of A431 cells with (right image) or without (left image) EGF stimulation, stained for caveolin-1 isoforms α and β (clone 2297). (B) Cluster densities of caveolin-1 α (clone 2234—solid bars) and caveolin-1 α and β (clone 2297—hatched bars) with (right panels) or without (left panels) EGF stimulation.

co-localization is less than 100% and therefore some of the receptors are outside the caveolae and some of the caveolae contain no receptors.

High magnification confocal images were collected and analyzed by ICCS to yield estimates of the density of receptor clusters, the density of caveolin clusters and the density of clusters that contain both receptor and caveolin (eqn. (7)). The percent of caveolin-1 co-localizing with the BMP or EGF receptors was estimated using eqn. (8). Fig. 3B shows that prior to stimulation with BMP-2 the fraction of co-localization of caveolin-1 α, as detected with clone 2234, and BRIa is about 20% (one fifth of the caveolae contain the receptor) and that after stimulation, the fraction of co-localization is about 34% (one third of the caveolae contain the receptor). Stimulation by BMP-2 increases the co-localization by about 43% ($p = 3.4 \times 10^{-7}$). In contrast, the co-localzation of caveolin-1 α and β, detected with clone 2297 and BRIa is not significantly affected BMP-2 stimulation remaining at about 26–27% ($p = 0.95$). The combination of these observations, increase in co-localization with caveolin-1 α and no change with both, indicates that less caveolin-1 β co-localizes with BRIa following stimulation with BMP-2. The implication is that BMP-2 stimulation may form caveolae enriched in the caveolin-1 α isoform and BRIa.

Fig. 3B also shows that BMP-2 stimulation does not significantly change the fraction of co-localization of caveolin-1 α and β with BRII, irrespective of which antibody is used to detect the

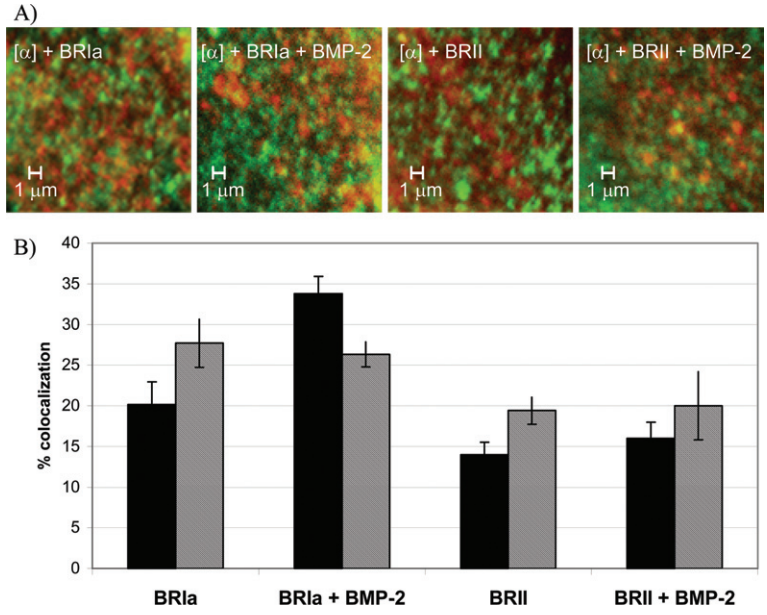

Fig. 3 Co-localization of caveolin-1 isoforms with BMP receptors. A431 cells were stimulated, or not stimulated, after serum starvation for 3 days with BMP-2, fixed and the BMP-receptors were labeled using polyclonal antisera against the BRIa or BRII and a secondary fluorescently labeled antibody. The same cells were labeled for caveolin-1 using an antibody specific for the α isoform [α] or for both α and β isoforms [αβ] and a secondary fluorescently labeled antibody. Cell membrane expression was visualized by confocal microscopy and forty images were collected at the highest magnification from forty different cells. (A) Sample confocal images showing colocalization of caveolin-1 α (clone 2234—green) with BRIa (red in the left two panels) and BRII (red in the right two panels) in the absence (images 1 and 3) or presence (images 2 and 4) of BMP-2. (B) The percent of caveolae with caveolin-1 α [α] (clone 2234—solid bars) or the fraction of caveolae with caveolin-1 α and β and caveolin β mainly [αβ] (clone 2297—hatched bars) that co-localize with BRIa (left two panels) and BRII (right two panels) in the absence (panels 1 and 3) or presence (panels 2 and 4) of BMP-2.

caveolin-1 (clone 2297 or clone 2234) ($p = 0.96$ for clone 2234 and $p = 0.98$ for clone 2297). This indicates that BRIa organization is more flexible than BRII on the cell surface..

Fig. 4B shows that EGF stimulation increases the co-localization of caveolin-1 α with ErbB1 by about 50% ($p = 2.93 \times 10^{-5}$). However, the co-localization of caveolin-1 α and β with ErbB1 is not changed significantly following EGF stimulation ($p = 0.62$). This observation is parallel to that observed for BRIa in Fig. 3B and the conclusion is equivalent: Stimulation of A431 cells by EGF causes the redistribution of caveolin-1 β into domains enriched in caveolin-1 α and the increase in caveolin-1 α co-localization with ErbB1 provides evidence for the existence of caveolae enriched in the caveolin-1 α isoform and ErbB1.

Overexpression of caveolin-1 beta leads to an inhibition of BMP signaling

Previous studies have shown that the interaction between the EGF receptor (ErbB1) and caveolin leads to inhibition of the kinase activity of the receptor. Since EGF stimulation causes a redistribution of caveolin-1 β it is possible that it is this isoform that specifically causes the inhibition and that the redistribution is intended to remove the inhibitory effect to allow signaling to take place. Since the BMP-2 and EGF stimulation cause the same effect, the first step is to determine whether there is inhibition of the BMP signaling when the interaction with the caveolin-1 β isoform is enhanced. Accordingly, we transfected the A431 cells with the caveolin-1 β isoform causing an overexpression. We then used a reporter gene assay to examine the influence of this overexpression on the activation of the Smad signaling pathway. Specifically, we co-transfected pSBE (with a *Renilla* luciferase construct) into A431 cells since the pSBE is known to be responsive to the activation of BMP signaling.[43] As Fig. 5 shows, BMP-2 stimulation leads to a four-fold increase in

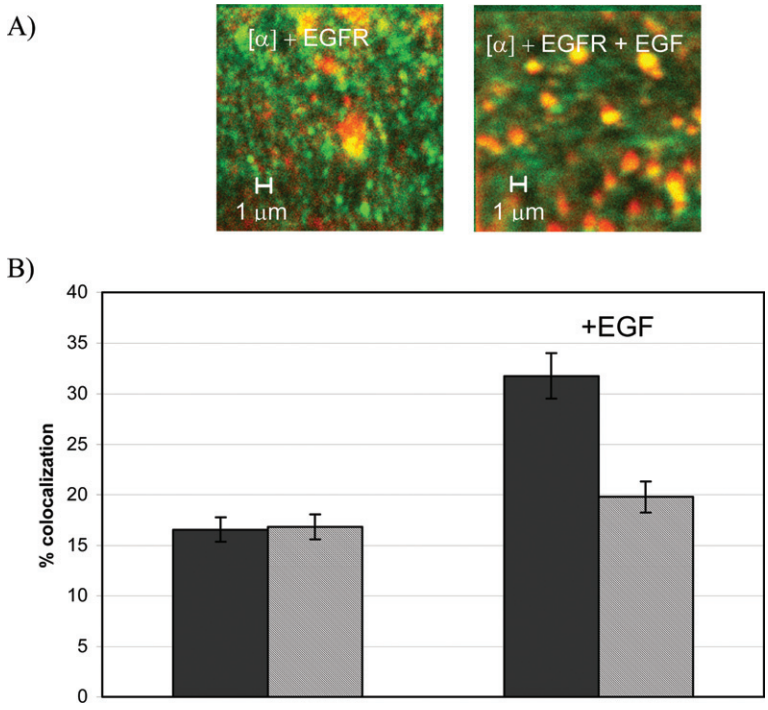

Fig. 4 Co-localization of caveolin-1 isoforms with EGF receptor. A431 cells were serum-starved for 72 h then stimulated or not with EGF and fixed. The EGF receptor was labeled using a polyclonal antibody recognizing the EGFR followed by a fluorescently tagged secondary antibody. The same cells were labeled for caveolin-1 using a monoclonal antibody specific for the α isoform [α] or for both α and β isoforms [αβ] and a secondary fluorescently labeled antibody. Cell membrane expression was visualized by confocal microscopy and forty images were collected at the highest magnification from forty different cells. (A) Sample confocal images showing colocalization of caveolin-1 α (clone 2234—green) with ErbB1 (red) in the absence (left image) or presence (right image) of EGF. (B) The percent of caveolae with caveolin-1 α [α] (clone 2234—solid bars) or the fraction of caveolae with caveolin-1 α and β and caveolin β mainly [αβ] (clone 2297—hatched bars) that co-localize with ErbB1 in the absence (left panel) or presence (right panel) of EGF.

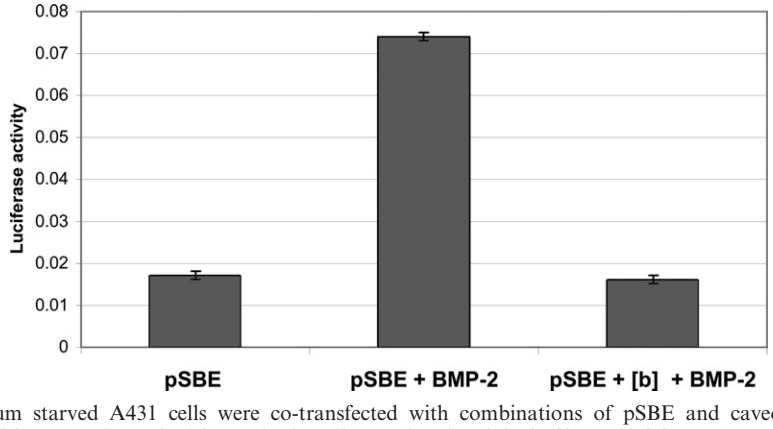

Fig. 5 Serum starved A431 cells were co-transfected with combinations of pSBE and caveolin-1 β and stimulated with BMP-2 for 12 h. After 12 h, the cells were lysed and the luciferase activity was measured. BMP-2 increases the luciferase activity by a factor of four (center bar) while co-transfection of caveolin-1 β prevents the BMP-2 induced luciferase activity (right bar) leaving it at basal levels (left bar). This shows that overexpression of caveolin-1 β leads to a complete inhibition of the Smad signaling pathway.

luciferase activity in these starved cells. However, co-expression of caveolin-1 β with the pSBE in A431 cells leads to a decrease in luciferase activity back to the level of unstimulated A431 cells even when they are stimulated with BMP-2. This suggests that the presence of excess caveolin-1 β isoform inhibits the BMP-2 signaling pathway. This is consistent with the previous studies on the ErbB1 that show that interaction of caveolin-1 with the EGF receptor inhibits receptor kinase activity, although in that work it was not attributed specifically to the caveolin-1 β isoform.[44]

Discussion

Caveolin-1 can exist as two isoforms differing in their N-terminus. There is evidence that these isoforms play different roles in caveolae formation.[9] Caveolae enriched in caveolin-1 β are shallower than caveolae containing both caveolin-1 α and β. In this work, we show that BMP and EGF receptors co-localize with these caveolin-1 isoforms in starved A431 cells to comparable extents. Stimulation of these starved A431 cells with either BMP-2 or EGF leads to comparable redistributions of caveolae enriched in the caveolin-1 β isoform into caveolae containing both caveolin-1 α and β isoforms. We are further able to show that the co-localization of BRIa with caveolae enriched in the caveolin-1 β isoform is decreased upon BMP-2 stimulation. Similarly, we show that stimulation with EGF leads to an increase in the co-localization of caveolin-1 α with ErbB1, whereas the co-localization of caveolin-1 α and β with ErbB1 remains unchanged. The cluster density of caveolin-1 α and β is decreased upon stimulation with BMP-2 or EGF, showing a redistribution of caveolin-1 β into domains enriched in caveolin-1 α. This provided new evidence for the existence of caveolae enriched in the caveolin-1 α isoform only. It is evident that the interaction of the receptors (BRIa and ErbB1) with the caveolin-1 isoforms is sensitive to the state of activation. The fact that both BMP-2 and EGF induce the same redistribution of caveolin-1 suggests that the phenomenon may be general and that the redistribution is functionally important in the signaling process.

We demonstrate that overexpression of the caveolin β isoform in starved A431 cells leads to an inhibition of BMP-2 induced signaling. This provides evidence that the caveolin-1 β isoform may inhibit signaling in caveolae enriched in the caveolin-1 β, suggesting that these caveolae may function to sequester the receptors in non-functional domains until they are needed, that is, they may act as storage units for the receptors. Upon stimulation, the receptors are released from the caveolin-1 β inhibitory effect as the caveolin-1 β redistributes.

It is known that BMP receptors can form preformed complexes between BRIa and BRII prior to BMP-2 binding, but these preformed complexes do not signal in the absence of BMP-2. Since BRII is a constitutively active kinase there must be a mechanism whereby the transphosphorylation of BRIa by BRII is silenced in the absence of BMP stimulation. It is possible that the caveolin-1 β enriched domains serve this function. In other words, the preformed complexes are inhibited by caveolin-1 β and the inhibition is released as a consequence of the redistribution of the caveolin-1 β in response to the BMP-2. An analogous inhibitory effect may be exerted on the ErbB1 receptor. Whatever the purpose, it is evident that there is an active and dynamic redistribution of caveolin-1 on the cell surface following BMP or EGF stimulation. This demonstrates that caveolae are dynamic structures on the cell surface whose composition may change to influence the signaling activity.

Acknowledgements

We want to thank NSERC and CIHR for providing the funding. We further acknowledge Dr D. W. Litchfield for helpful discussions and providing access to certain equipment and space.

References

1 R. G. Parton, *Curr. Opin. Cell. Biol.*, 1996, **8**, 542–548.
2 R. G. W. Anderson, *Annu. Rev. Biochem.*, 1998, **67**, 199–225.
3 T. Fujimoto, H. Hagiwara, T. Aoki, H. Kogo and R. Nomura, *J. Electron Microsc.*, 1998, **47**, 451–460.
4 K. G. Rothberg, J. E. Heuser, W. C. Donzell, Y. S. Ying, J. R. Glenney and R. W. G. Anderson, *Cell*, 1992, **68**, 673–682.

5 P. E. Scherer, T. Okamoto, M. Chun, I. Nishimoto, H. F. Lodish and M. P. Lisanti, *Proc. Natl. Acad. Sci. USA*, 1996, **93**, 131–135.
6 Z. Tang, P. E. Scherer, T. Okamoto, K. Song, C. Chu, D. S. Kohtz, I. Nishimoto, H. F. Lodish and M. P. Lisanti, *J. Biol. Chem.*, 1996, **27**, 2255–2261.
7 P. E. Scherer, Z. Tang, M. Chun, M. Sargiacomo, H. F. Lodish and M. P. Lisanti, *J. Biol. Chem.*, 1995, **270**, 16 395–16 401.
8 A. Schlegel and M. P. Lisanti, *Cytokine Growth Factor Rev.*, 2001, **12**, 41–51.
9 T. Fujimoto, H. Kogo, R. Nomura and T. Une, *J. Cell Sci.*, 2000, **113**, 3509–3517.
10 B. L. Hogan, *Genes Dev.*, 1996, **10**, 1580–1594.
11 M. Bhatia, D. Bonnet, D. Wu, B. Murdoch, J. Wrana, L. Gallacher and J. E. Dick, *J. Exp. Med.*, 1999, **189**, 1139–48.
12 A. J. Celeste, J. A. Iannazzi, R. C. Taylor, R. M. Hewick, V. Rosen, E. A. Wang and J. M. Wozney, *Proc. Natl. Acad. Sci. USA*, 1990, **87**, 9843–9847.
13 N. S. Cunningham, N. A. Jenkins, D. J. Gilbert, N. G. Copeland, A. H. Reddi and S. J. Lee, *Growth Factors*, 1995, **12**, 99–109.
14 E. E. Storm, T. V. Huynh, N. G. Copeland, N. A. Jenkins, D. M. Kingsley and S. J. Lee, *Nature*, 1994, **368**, 639–643.
15 N. R. Dunn, G. E. Winnier, L. K. Hargett, J. J. Schrick, A. B. Fogo and B. L. Hogan, *Dev. Biol.*, 1997, **188**, 235–247.
16 R. W. Padgett, R. D. St. Johnson and W. M. Gelbert, *Nature*, 1987, **325**, 81–84.
17 M. Kretzschmar, J. Doody and J. Massague, *Nature*, 1997, **389**, 618–22.
18 J. Massague, *Annu. Rev. Biochem.*, 1998, **67**, 753–791.
19 P. A. Hoodless, T. Haerry, S. Abdollah, M. Stapleton, M. B. O'Connor, L. Attisano and J. L. Wrana, *Cell*, 1996, **85**, 489–500.
20 M. Kawabata, A. Chytil and H. L. Moses, *J. Biol. Chem.*, 1995, **270**, 5625–5630.
21 F. Liu, F. Ventura, J. Doody and J. Massague, *Mol. Cell. Biol.*, 1995, **15**, 3479–3486.
22 T. Nohno, T. Ishikawa, T. Saito, K. Hosokawa, S. Noji, D. H. Wolsing and J. S. Rosenbaum, *J. Biol. Chem.*, 1995, **270**, 22 522–22 526.
23 B. L. Rosenzweig, T. Imamura, T. Okadome, G. N. Cox, H. Yamashita, P. ten Dijke, C. H. Heldin and K. Miyazono, *Proc. Natl. Acad. Sci. USA*, 1995, **92**, 7632–7636.
24 L. Attisano and J. L. Wrana, *Curr. Opin. Cell Biol.*, 2000, **12**, 235–243.
25 N. Kimura, R. Matsuo, H. Shibuya, K. Nakashima and T. Taga, *J. Biol. Chem.*, 2000, **23**, 17 647–52.
26 K. Shirakabe, K. Yamaguchi, H. Shibuya, K. Irie, T. Moriguchi, Y. Gotoh, K. Matsumo and E. Nishoda, *J. Biol. Chem.*, 1997, **272**, 8141–8144.
27 K. Nakamura, T. Shirai, S. Morishita, S. Uchida, K. Saeki-Miura and F. Makishima, *Exp. Cell Res.*, 1999, **250**, 351–63.
28 A. Nohe, S. Hassel, M. Ehrlich, F. Neubauer, W. Sebald, Y. Henis and P. Knaus, *J. Biol. Chem.*, 2002, **15**, 5330–829.
29 N. Prenzel, O. M. Fischer, S. Streit, S. Hart and A. Ullrich, *Endocrine-Related Cancer*, 2001, **8**, 11–31.
30 D. J. Riese and D. Stern, *BioEssays*, 1998, **20**, 41–48.
31 R. N. Jorissen, F. Walker, N. Pouliot, T. P. J. Garrett, C. W. Ward and A. W. Burgess, *Exp. Cell Res.*, 2003, **6**, 31–53.
32 C. M. Brown, M. G. Roth, Y. I. Henis and N. O. Petersen, *Biochemistry*, 1999, **38**, 15 166–73.
33 C. M. Brown and N. O. Petersen, *J. Cell Sci.*, 1998, **111**, 271–81.
34 M. Srivastava and N. O. Petersen, *Biophys. Chem.*, 1998, **75**, 201–11.
35 P. W. Wiseman and N. O. Petersen, *Biophys. J.*, 1999, **76**, 963–77.
36 P. W. Wiseman, P. Hoddelius, N. O. Petersen and K. E. Magnusson, *FEBS Lett.*, 1997, **401**, 43–8.
37 N. O. Petersen, in *Fluorescence Correlation Spectroscopy*, ed. R. Rigler and E. S. Elson, Springer–Verlag, Berlin, Heidelberg, New York, 2001.
38 A. Nohe and N. O. Petersen, *Biophotonics*, 2002, **9**, 39–52.
39 N. O. Petersen, C. Brown, A. Kaminski, J. Rocheleau, M. Srivastava and P. Wiseman, *Faraday Discuss.*, 1998, **111**, 289–305.
40 B. J. Berne and R. Pecora, *Dynamic Light Scattering with Applications to Chemistry, Biology and Physics*, J. Wiley, New York, 1995.
41 P. W. Wiseman, P. Hoddelius, N. O. Petersen and K. E. Magnusson, *FEBS Lett.*, 1997, **401**, 43–8.
42 A. Nohe, E. Keating, T. M. Underhill, P. Knaus and N. O. Petersen, *J. Cell Sci.*, 2003, **116**, 3277–3284.
43 L. J. C. Jonk, S. Itoh, C.-H. Heldin, P. ten Dijke and W. Kruijer, *J. Biol. Chem.*, 1998, **273**, 21 145–21 152.
44 J. Couet, M. Sargiacomo and M. P. Lisanti, *J. Biol. Chem.*, 1997, **272**, 30 429–30 438.